Journal of Inherited Metabolic Disease

WILEY

JIMD SSIEM

ORIGINAL ARTICLE OPEN ACCESS

Liver-Directed Gene Therapy Mitigates Early Nephropathy in Murine Glycogen Storage Disease Type Ia

Cheol Lee[1] | Kunal Pratap[1] | Lisa Zhang[1] | Hung Dar Chen[1] | Irina Arnaoutova[1] | Matthew F. Starost[2] | Brian C. Mansfield[1] | Janice Y. Chou[1]

[1]Section on Cellular Differentiation, Division of Translational Medicine, Eunice Kennedy Shriver National Institute of Child Health and Human Development, Bethesda, Maryland, USA | [2]Division of Veterinary Resources, National Institutes of Health, Bethesda, Maryland, USA

Correspondence: Janice Y. Chou (chouja@mail.nih.gov)

Received: 24 February 2025 | **Revised:** 8 May 2025 | **Accepted:** 13 May 2025

Communicating Editor: Carlos R. Ferreira

Funding: This work was supported by the Intramural Research Program of the *Eunice Kennedy Shriver* National Institute of Child Health and Human Development(HD000912-38), National Institutes of Health (https://intramural.nih.gov/search/searchview.taf).

Keywords: fibrosis | glucose homeostasis | glucose reabsorption | glucose-6-phosphatase-α | mouse model

ABSTRACT

Nephropathy is a complication of glycogen storage disease type Ia (GSD-Ia), a metabolic disorder caused by pathogenic variants in glucose-6-phosphatase-α (G6Pase-α or G6PC1). While maintaining blood glucose homeostasis can delay the progression of renal disease in GSD-Ia, the benefits of liver-directed G6PC1 gene therapy on nephropathy remain unclear. This study evaluates the effects of low- and high-dose G6PC1 liver gene augmentation therapy on kidney function. The *G6pc*−/− mice, which lack G6Pase-α activity in both liver and kidney, were treated with G6PC1 gene therapy to restore either low or near-normal levels of liver G6Pase-α activity, and renal phenotype was examined at age 12 weeks. Both groups exhibited impaired renal glucose homeostasis, altered renal glucose reabsorption, acute kidney injury, and early signs of renal fibrosis. However, mice with near-normal liver G6Pase-α activity had better renal glucose reabsorption and homeostasis with lower serum levels of cystatin C and blood urea nitrogen, key markers of kidney function. These findings highlight the potential of liver-directed G6PC1 gene therapy to enhance metabolic control and mitigate early kidney disease in GSD-Ia.

1 | Introduction

Glycogen storage disease type Ia (GSD-Ia; MIM 232200) is an autosomal recessive metabolic disorder caused by a deficiency in glucose-6-phosphatase-α (G6Pase-α or G6PC1) [1–3]. Between meals, G6Pase-α dephosphorylates glucose-6-phosphate (G6P), the product of glycogenolysis and gluconeogenesis, to release glucose into the blood to maintain euglycemia [1–3]. Liver dysfunction in GSD-Ia patients results in fasting hypoglycemia, which is neonatally fatal without dietary therapies [4–6], while kidney dysfunction results in nephropathy [1–3]. Liver function is therefore the primary concern in treating GSD-Ia. Several liver-directed G6PC1 gene therapies have shown clinical promise [7], including a completed phase III trial for G6PC1 gene augmentation (NCT05139316) currently under Food and Drug Administration review, and an ongoing phase I/II clinical trial for mRNA augmentation (NCT05095727). Additionally,

Abbreviations: Ang, angiotensin; AGT, angiotensinogen; AKI, acute kidney injury; BMI, body mass index; BUN, blood urea nitrogen; BW, body weight; CTGF, Connective tissue growth factor; DAB, 3,3-diaminobenzidine; Dkk3, Dickkopf-3; ECM, extracellular matrix; EMT, epithelial-to-mesenchymal transition; G6P, glucose-6-phosphate; G6Pase-α, glucose-6-phosphatase-α; *G6pc*−/−, *G6pc*-deficient; GLUT, glucose transporter; GSD-Ia, glycogen storage disease type Ia; H&E, hematoxylin and eosin; KW, kidney weight; HRP, horseradish peroxidase; RAS, renin-angiotensin system; SGLT, sodium-glucose cotransporter; α-SMA, α-smooth muscle actin; TCF/LEF, T-cell factor/lymphoid enhancer-binding factor.

an adenine base editor gene-editing strategy targeting the most prevalent *G6PC1* mutation has demonstrated preclinical efficacy [7, 8] and recently entered phase I/II clinical trials (NCT06735755).

The rAAV8-G6PC1 vector used in gene augmentation selectively targets the liver and does not transduce the kidney [9]. Similarly, lipid nanoparticles delivering the adenine base editor [8] and mRNA primarily accumulate in hepatocytes within the liver [10]. Consequently, developing effective kidney-targeted therapies remains challenging. Previous studies suggest that strict dietary management can help delay the progression of renal disease [11]. This study investigates whether liver-directed G6PC1 gene augmentation alone can also improve early kidney disease in GSD-Ia.

The *G6pc*−/− (GSD-Ia) mice [12] mimic human GSD-Ia, exhibiting impaired renal gluconeogenesis, altered renal glucose reabsorption, acute kidney injury (AKI), and renal fibrosis [13]. Fewer than 30% *G6pc*−/− mice survive beyond weaning, even with a glucose therapy [12], and at 3 weeks of age early-stage renal dysfunction is not detectable [13] via serum marker analysis [14], necessitating studies in older mice. To address this, we developed a liver G6Pase-α augmented (L-G6PC1), kidney G6Pase-α null (K^{null}) model for nephropathy studies [13]. These mice received liver-directed G6PC1 gene therapy [9] at 2 weeks of age, which is sufficient to provide long-term blood glucose homeostasis and survival [7, 15, 16]. To study the impact of restoration of liver-specific G6Pase-α on GSD-Ia nephropathy, we generated two groups of liver augmented GSD-Ia mice: one expressing 86% of normal liver G6Pase-α activity (L-G6PC1-high) and another expressing 2% of normal liver G6Pase-α activity (L-G6PC1-low). Since the mouse background is a global G6PC1 knockout, the liver augmented mice lack kidney G6Pase-α expression [13].

In this study, we treated *G6pc*−/− mice with liver-directed G6PC1 gene augmentation [9] at 2 weeks of age and assessed nephropathy 10 weeks later. While both L-G6PC1-high and L-G6PC1-low groups exhibited similar renal pathology, higher liver G6Pase-α activity improved renal glucose homeostasis and reabsorption. Mice with low hepatic G6Pase-α activity showed significant lipid accumulation in glomerular and tubular cells, contributing to nephropathy [17, 18], whereas those with near-normal activity maintained normal renal triglyceride levels. Serum marker analysis [14] also indicated a slower decline in kidney function with higher liver G6Pase-α activity. These findings suggest that liver-directed G6PC1 gene therapy enhances renal metabolic control and mitigates early nephropathy in GSD-Ia.

2 | Materials and Methods

2.1 | Animals

All animal studies were conducted under an animal protocol approved by the *Eunice Kennedy Shriver* National Institute of Child Health and Human Development Animal Care and Use Committee. All institutional and national guidelines for the care and use of laboratory animals were followed. The animal experiments abide by the ARRIVE guidelines (https://arriveguidelines.org/arrive-guidelines). Mice were maintained on a standard NIH-31 Open formula mouse/rat sterilizable diet (Envigo) without any restrictions. Mice were housed at the animal facility in a 12-h light/dark cycle, with an ambient temperature controlled within 65°F–75°F (18°C–24°C) and a humidity level between 40% and 60%. To reduce feeding competition between littermate pups, the size of the litter was usually reduced to 6–8 pups.

A G6PC1-expressing recombinant adeno-associated virus serotype-2/8 vector (rAAV8-G6PC1) that targets the liver but not the kidney [9] was used to restore hepatic G6PC1 expression in the *G6pc*−/− mice [12]. The L-G6PC1-low and L-G6PC1-high mice, lacking kidney G6Pase-α activity, were generated by treating 2-week-old *G6pc*−/− mice with 1×10^{12} or 4×10^{13} vp/kg of rAAV8-G6PC1, respectively. We have shown that *G6pc*−/− mice titrated with rAAV-G6PC1 to express 3–5 units of hepatic G6Pase-α activity survive long-term and maintain glucose homeostasis [15, 16]. As expected, both L-G6PC1-low and L-G6PC1-high mice survived adulthood without hypoglycemic seizures. The age-matched *G6pc*+/+ and *G6pc*+/− mice, which have a wild-type phenotype, were used as controls.

The body mass index (BMI) was calculated by dividing the body weight measured in grams by the square of the body length measured in cm. The body length of each mouse was measured as the distance from the tip of the nose to the base of the tail.

2.2 | Phosphohydrolase Assays

Liver microsome isolation and microsomal phosphohydrolase assays were performed as described previously [12]. Permeabilized microsomes were prepared by incubating intact microsomes in sucrose buffer containing 0.2% sodium deoxycholate for 20 min on ice. In phosphohydrolase assays, reaction mixtures (50 μL) containing 50 mM sodium cacodylate buffer, pH 6.5, 2 mM EDTA, 10 mM G6P, and 100–200 μg of permeabilized microsomes were incubated at 30°C for 10 min. The background of non-specific phosphatase activity was estimated by pre-incubating permeabilized microsomes in 20 mM sodium acetate buffer, pH 5, for 10 min at 37°C to inactivate the acid-labile G6Pase-α. One unit of G6Pase-α activity represents 1 nmol G6P hydrolysis per minute per mg microsomal protein. The background of non-specific phosphatase activity varied in the lysates from 0.2 to 2 units. The background was subtracted from all data points.

Enzyme histochemical analysis of G6Pase-α was performed on cryopreserved OCT embedded kidney sections as described [15]. Briefly, 10 μm thick tissue sections were incubated at room temperature for 10 min in a reaction buffer containing 40 mM Tris-maleate pH 6.5, 10 mM G6P, 300 mM sucrose, and 3.6 mM lead nitrate, followed by 2 washes in 300 mM sucrose solution. Then, the tissue sections were incubated for 2 min at room temperature in 0.09% ammonium sulfide solution, and the trapped lead phosphate was visualized following conversion to the brown colored lead sulfide. Images of the tissue sections were taken by the Imager A2m microscope with

Axiocam 506 camera and the ZEN 2.6 software (Carl Zeiss, White Plains, NY).

2.3 | Renal Metabolite Analysis, Hematoxylin and Eosin, Oil Red O, and Masson's Trichrome Staining

Mouse kidneys were homogenized in 5% NP-40, incubated at 99°C for 5 min, and centrifuged to remove insoluble materials. The resulting supernatants were used to measure levels of G6P, lactate, triglyceride, and glycogen using the respective assay kits from Abcam (Waltham, MA, USA).

Hematoxylin and eosin (H&E) and Masson's trichrome staining were performed on paraffin-embedded mouse kidney sections. Oil Red O staining was performed on cryopreserved OCT-embedded kidney sections. The stained sections were scanned and visualized using the Zeiss Axioscan Z1 and Imager A2m microscope with an Axiocam 506 camera and the ZEN 3.8 software (Carl Zeiss, White Plains, NY).

2.4 | Western-Blot Analysis

Western-blot images were detected using the LI-COR Odyssey scanner and analyzed using the Image Studio 5.5 software (Li-Cor Biosciences, Lincoln, NE). The antibodies used were: Abcam (Cambridge, MA), CTGF (ab6992); Cell Signaling Technology (Danvers, MA), rabbit β-actin (#4970), β-catenin (#8480), non-phosphorylated β-catenin (#8814), α-SMA (#14968), E-cadherin (#3195), N-cadherin (#13116), Snail1 (#3879), and collagen-Iα1 (#72026); Immuno-Biological Laboratories (Minneapolis, MN, USA), Angiotensinogen (28101); LS Bio (Seattle, WA, USA), collagen-IV (LS-B8763); MyBioSource (San Diego, CA); Dkk3 (MBS840225) and SGLT2 (MBS821113); Santa Cruz Biotechnology (Dallas, TX), mouse β-actin (sc-47 778) and renin (sc-133 145); Thermo Fisher Scientific (Waltham, MA), GLUT2 (MA5-35162).

2.5 | Immunohistochemical Analysis

Nuclear-translocated active β-catenin was analyzed by immunohistochemistry on paraffin-embedded mouse kidney sections using a rabbit monoclonal antibody specific for non-phosphorylated (active) β-catenin (#8814, Cell Signaling Technology). This was followed by incubation with horseradish peroxidase (HRP)-conjugated anti-rabbit secondary antibody. DAB substrate (3,3′-diaminobenzidine) was then added, which was converted by HRP into a brown-colored product. Sections were counterstained with hematoxylin to visualize nuclei in blue. The immunostained kidney sections were digitized using the Motic EasyScan Infinity 60 (Motic Digital Pathology, Emeryville, CA, USA) and subsequently analyzed with QuPath software v0.4.3 [19]. To further subclassify β-catenin nuclear staining, intensity thresholds were established based on mean nuclear hematoxylin optical densities, categorizing nuclei as negative, weak, moderate, or strongly positive. For quantification purposes, only nuclei classified as moderate or strongly positive were included.

2.6 | Serum Cystatin C, Creatinine, Blood Urea Nitrogen, and Metabolites Analysis

Blood was collected by cardiac puncture of the non-fasted, mice at sacrifice. Blood was transferred into MiniCollect TUBE 0.8 mL CAT Serum Separator (#450472, Greiner Bio-one), allowed to coagulate for 20 min, then centrifuged for 10 min at 2000*g*. Serum was transferred to a new microtube, flash-frozen in liquid nitrogen, and stored at −80°C. Serum creatinine was determined using the Mouse Creatinine Assay Kit (#MBS763433) from MyBioSource (San Diego, CA), serum cystatin C was determined using the Mouse/Rat Cystatin C Quantikine ELISA Kit (#MSCTC0) from R&D Systems (Minneapolis, MN), and serum blood urea nitrogen (BUN) was determined using the Urea Nitrogen (BUN) Colorimetric Detection Kit (#EIABUN) from Thermo Fisher Scientific (Asheville, NC).

Serum triglycerides (ab65336), cholesterol (ab65359), and uric acid (ab65344) were analyzed using their respective kits from Abcam. Serum lactate was measured using the EnzyChrom D-Lactate Assay Kit (EDLC-100) from BioAssay Systems (Hayward, CA).

2.7 | Statistical Analysis

The statistical analyzes reported are one-way ANOVA followed by Tukey's post hoc comparison tests performed using the GraphPad Prism Program, version 10.2.2 (GraphPad Software, San Diego, CA). Data are presented as Mean values ± SEM, and individual data points for each animal are displayed. * denotes $p < 0.05$, ** denotes p value < 0.005.

3 | Results

3.1 | Renal Glucose Homeostasis in L-G6PC1-Low and L-G6PC1-High Mice

To evaluate whether liver-directed gene therapy can improve GSD-Ia nephropathy, 2-week-old *G6pc*−/− mice were treated with either a low (1×10^{12} vp/kg) or high (4×10^{13} vp/kg) dose of rAAV8-G6PC1, generating the L-G6PC1-low and L-G6PC1-high mouse models, respectively. At 12 weeks of age, the average hepatic G6Pase-α activity in age-matched mice was 239.7 ± 18 units for control, 4.8 ± 1.3 units (2.3% of control) for L-G6PC1-low, and 206.1 ± 14 units (86.0% of control) for L-G6PC1-high (Figure 1A).

We have demonstrated previously that rAAV8-G6PC1 selectively targets the liver without transducing the kidney [9]. To confirm that L-G6PC1-high mice receiving 4×10^{13} vp/kg of rAAV8-G6PC1 remained G6PC1-null in the kidney, we examined G6Pase-α expression using enzyme histochemical analysis. As expected, high G6Pase-α expression was detected in the kidney cortex of control littermates but was undetectable in kidney sections from 3-week-old *G6pc*−/− mice as well as the rAAV-G6PC1 treated L-G6PC1-low and L-G6PC1-high mice (Figure 1B).

These G6Pase-α activity levels resulted in blood glucose concentrations of 104.4 ± 8.8 mg/dL (70.1% of control) for L-G6PC1-low mice and 135.1 ± 2.8 mg/dL (90.8% of control) for

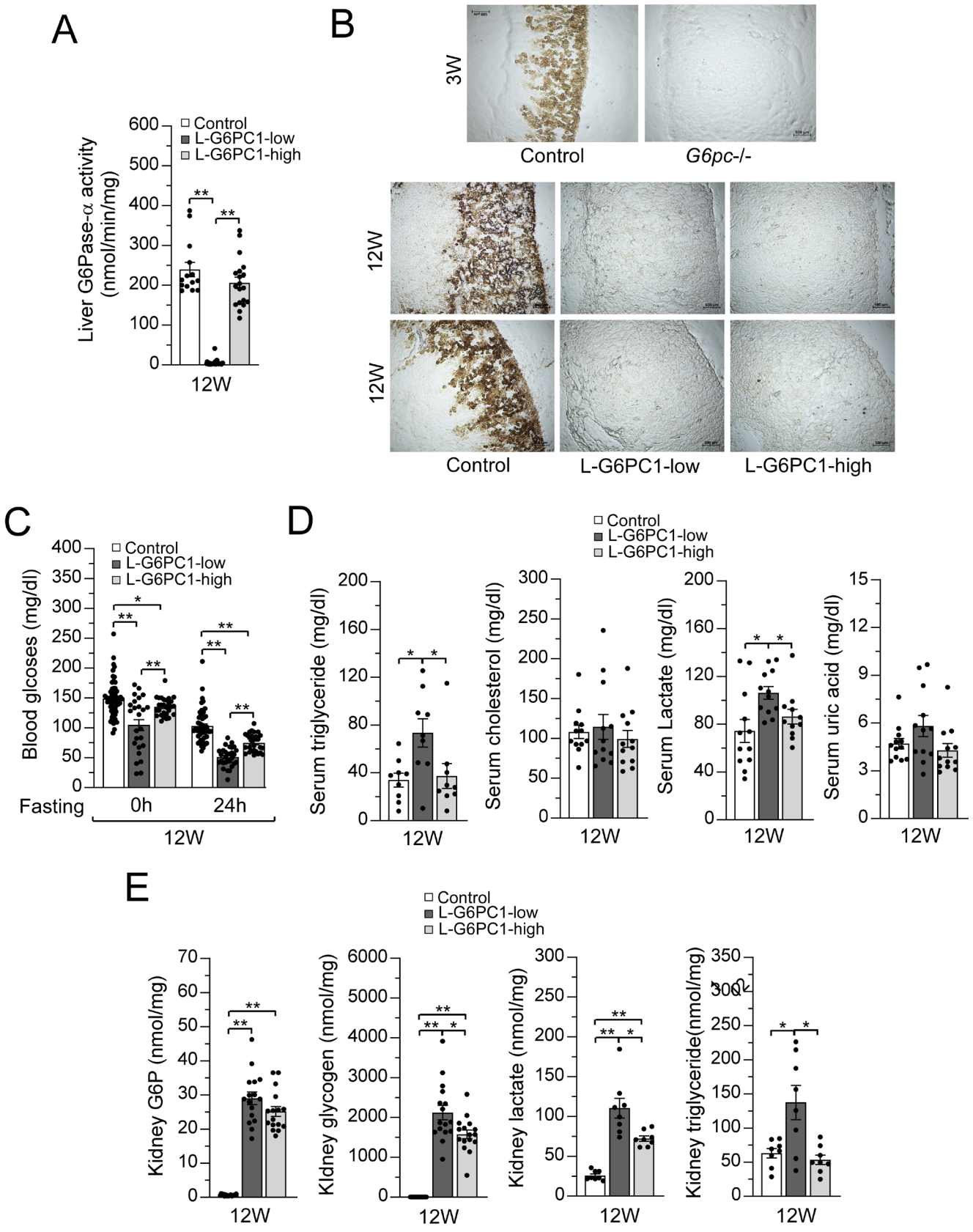

FIGURE 1 | Legend on next page.

L-G6PC1-high mice, both sufficient for viable glycemia but statistically lower than those of control littermates. Blood glucose levels are primarily regulated by the liver and kidney, with the liver contributing 75%–80% of glucose production during fasting [20, 21]. After 24 h of fasting, blood glucose levels declined as expected but maintained a similar relationship, at 49.5% control for L-G6PC1-low and 72.7% for L-G6PC1-high mice (Figure 1C).

FIGURE 1 | The phenotype of L-G6PC1-low and L-G6PC1-high mice. L-G6PC1-low and L-G6PC1-high mice were generated from *G6pc*−/− mice and analyzed at 12 weeks of age. Age-matched *G6pc*+/+ and *G6pc*+/− mice with a similar phenotype served as controls. (A) Liver microsomal G6Pase-α activity in control ($n = 14$), L-G6PC1-low ($n = 30$), and L-G6PC1-high ($n = 19$) mice. (B) Enzyme histochemical analysis of G6Pase-α in the kidneys of 3-week-old *G6pc*−/− and control mice ($n = 3$ per group) as well as in 12-week-old L-G6PC1-low and L-G6PC1-high mice and age-matched control littermates ($n = 6$ per group). (C) Fasting blood glucose levels in 12-week-old control ($n = 58$), L-G6PC1-low ($n = 26$), and L-G6PC1-high ($n = 28$) mice. (D) Serum triglycerides ($n = 9$ per group), cholesterol ($n = 12$ per group), lactate ($n = 12$ per group), and uric acid ($n = 12$ per group) in 12-week-old control, L-G6PC1-low, and L-G6PC1-high mice. (E) Kidney G6P ($n = 16$ per group), glycogen ($n = 16$ per group), lactate ($n = 8$ per group), and triglyceride ($n = 8$ per group) levels in 12-week-old control, L-G6PC1-low, and L-G6PC1-high mice. Values represent the mean ± SEM. $^*p < 0.05$, $^{**}p < 0.005$.

Compared to 12-week-old control mice, serum levels of triglyceride and lactate were elevated in L-G6PC1-low mice but remained statistically unchanged in L-G6PC1-high mice (Figure 1D), suggesting that liver G6Pase-α activity may modulate serum levels of triglyceride and lactate. In contrast, serum levels of cholesterol and uric acid were similar across control, L-G6PC1-low, and L-G6PC1-high mice (Figure 1D).

In the absence of kidney G6Pase-α activity, G6P accumulates in the kidney cytoplasm, leading to increased glycogen synthesis and enhanced glycolysis [22]. In 12-week-old mice, kidney G6P levels averaged 0.62 ± 0.06 nmol/mg in control mice, 29.1 ± 1.86 nmol/mg in L-G6PC1-low mice, and 25.18 ± 1.48 nmol/mg in L-G6PC1-high mice (Figure 1E). However, the difference in kidney G6P levels between L-G6PC1-low and L-G6PC1-high mice was not statistically significant. Kidney glycogen storage followed a slightly different pattern. While control mice exhibited very low kidney glycogen levels (0.45 ± 0.05 nmol/mg), the absence of kidney G6Pase-α led to a dramatic increase in glycogen accumulation: 2124 ± 183 nmol/mg in L-G6PC1-low mice and 1577 ± 110 nmol/mg in L-G6PC1-high mice. These values represent 4720-fold and 3504-fold increases, respectively, compared to controls (Figure 1E). Notably, the 26% reduction in glycogen storage observed in L-G6PC1-high mice compared to L-G6PC1-low mice was statistically significant, suggesting that liver G6Pase-α activity may influence kidney glycogen storage.

A more significant finding was the impact of increased liver G6Pase-α activity on renal glycolysis (Figure 1E). Both L-G6PC1-low and L-G6PC1-high mice exhibited increased kidney lactate production, indicating enhanced renal glycolysis compared to control mice. However, renal lactate levels were significantly higher in L-G6PC1-low mice than in L-G6PC1-high mice (Figure 1E). Enhanced renal glycolysis can also promote triglyceride production. Interestingly, compared to control mice, renal triglyceride levels increased only in L-G6PC1-low mice (Figure 1E). In contrast, L-G6PC1-high mice maintained statistically normal triglyceride levels, suggesting markedly improved glycolysis. Oil Red O staining further confirmed that neutral fat deposits were primarily elevated in L-G6PC1-low mice (Figure 2A).

Nephromegaly, as indicated by increased kidney weight (KW) to body weight (BW) ratios compared to controls, is an early clinical manifestation of renal disease in GSD-Ia and was observed in both L-G6PC1-low and L-G6PC1-high mice (Figure 2B). Notably, the KW/BW ratio was statistically higher in L-G6PC1-low compared to L-G6PC1-high mice, correlating with the differences seen in renal glycogen accumulation.

Previous studies on *G6pc*−/− mice have demonstrated that rAAV-G6PC1 gene therapy supports long-term survival (≥ 1 year) [15, 16] and protects against age-related obesity, as measured by BMI [23]. In the present study, at 12 weeks of age, BMI values showed a statistically significant reduction in both L-G6PC1-low and L-G6PC1-high mice, with L-G6PC1-high mice exhibiting a small but significant decrease compared to L-G6PC1-low mice (Figure 2C). This trend suggests that, in the absence of renal G6Pase-α expression in G6PC1/K^{null} mice, hepatic G6Pase-α plays a crucial role in maintaining metabolic control.

H&E staining revealed significant glycogen accumulation in both 12-week-old G6PC1-low and G6PC1-high mice (Figure 2D). This accumulation led to the swelling of epithelial cells in the proximal convoluted cortical tubules and multiple glomerular Bowman's capsule parietal epithelial cells. Additionally, the cortex exhibited mild to moderate tubular dilation, which was more pronounced in the G6PC1-low mice compared to the G6PC1-high mice. These findings also suggest that restoring liver expression of G6Pase-α activity can ameliorate the severity of kidney pathology and that higher levels of augmentation may be more beneficial.

3.2 | L-G6PC1-High Mice Display Improved Renal Glucose Reabsorption

The kidney proximal tubules play a key role in glucose homeostasis, undertaking endogenous glucose production via gluconeogenesis and glucose reabsorption mediated by GLUT2 and SGLT2 [24–26]. Consistent with previous findings in 3-week-old *G6pc*−/− mice [13], we observed increased GLUT2 protein levels and decreased SGLT2 protein levels in the kidneys of both 12-week-old L-G6PC1-low and L-G6PC1-high mice, compared to the age-matched control littermates (Figure 2E). Notably, increasing liver G6Pase-α expression in the G6PC1/K^{null} mice reduced the overexpression of kidney GLUT2 and increased expression of kidney SGLT2, bringing both closer to the control levels, suggesting hepatic G6Pase-α expression benefits renal glucose reabsorption in a G6Pase-α null kidney.

3.3 | The L-G6PC1-High and L-G6PC1-Low Mice Display AKI

We previously demonstrated that increased renal glycogen accumulation, impaired renal glucose homeostasis, and altered renal glucose reabsorption contribute to AKI in 3-week-old *G6pc*−/− mice [13]. To investigate further, we analyzed the expression of N-cadherin, a cell adhesion molecule whose levels decrease during AKI [27], and Dickkopf-3 (Dkk3) [28, 29], a pro-fibrotic glycoprotein marker of AKI synthesized by stressed renal tubular epithelial cells. Both L-G6PC1-low and L-G6PC1-high

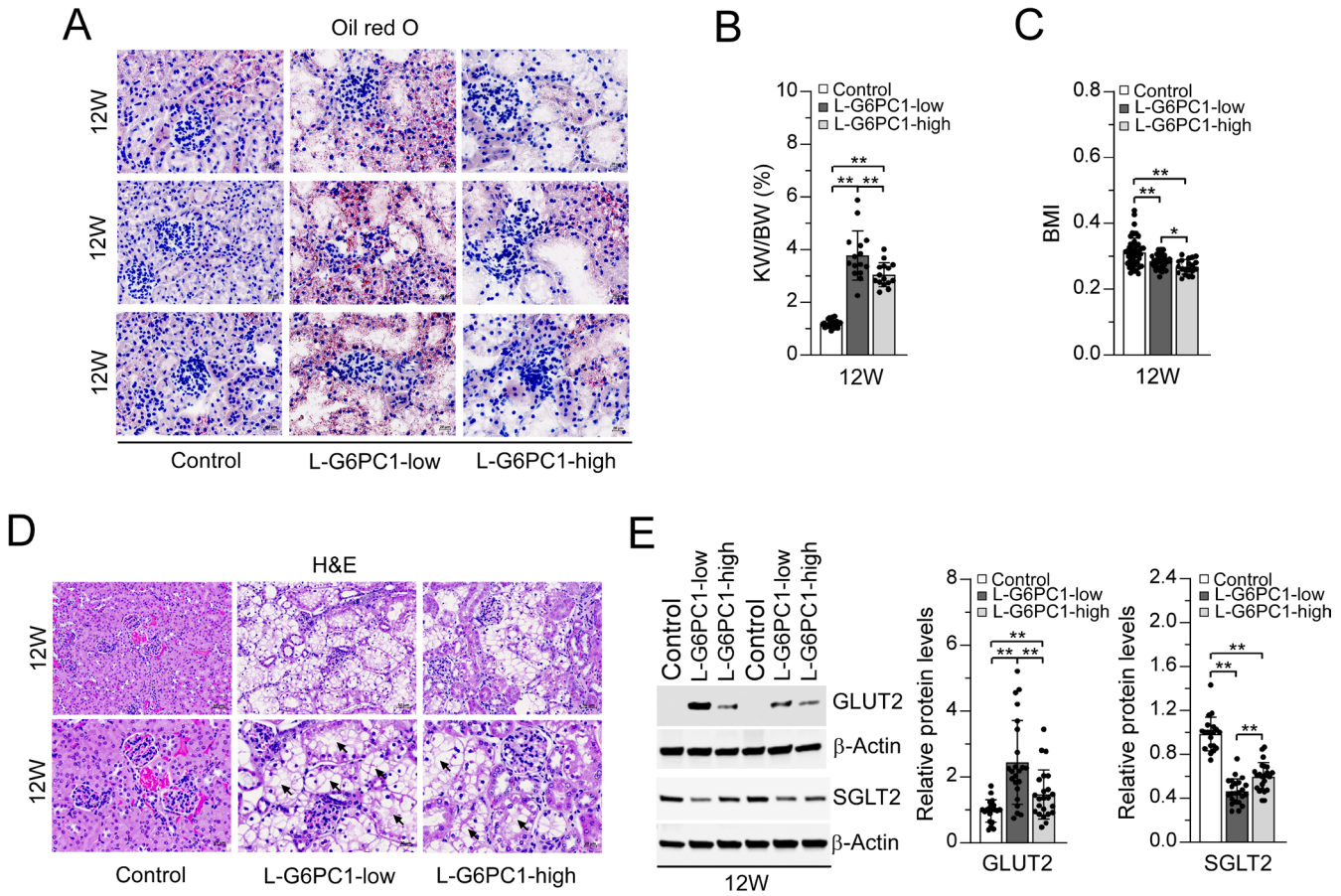

FIGURE 2 | Assessment of kidney glucose homeostasis, reabsorption and early injury in L-G6PC1-low and L-G6PC1-high mice. L-G6PC1-low and L-G6PC1-high mice were generated from *G6pc*−/− mice and analyzed at 12 weeks of age. Age-matched *G6pc*+/+ and *G6pc*+/− mice with a similar phenotype served as controls. (A) Oil Red O (neutral triglycerides and lipids) staining of the kidneys in control ($n=6$), L-G6PC1-low ($n=6$), and L-G6PC1-high ($n=6$) mice. Three sets of representative staining are shown for each group of mice. Scale bar, 20 μm. (B) Ratio of kidney weight (KW) to body weight (BW) in control ($n=26$), L-G6PC1-low ($n=15$), and L-G6PC1-high ($n=15$) mice. (C) Body mass index (BMI) in control ($n=50$), L-G6PC1-low ($n=29$), and L-G6PC1-high ($n=20$) mice. (D) H&E staining of the kidneys in control ($n=6$), L-G6PC1-low ($n=6$), and L-G6PC1-high ($n=6$) mice at magnifications of x200 (top panels, Scale bar, 50 μm) and x400 (lower panels, Scale bar, 20 μm), Arrows point to the area of tubular dilation. Representative sets of staining are shown. (E) Western-blot analyzes and quantitation of renal levels of GLUT2 and SGLT2 in control ($n=20$), L-G6PC1-low ($n=23$), and L-G6PC1-high ($n=23$) mice. Densitometric quantification was performed and normalized against β-Actin. Values represent the mean ± SEM. $^{*}p<0.05$, $^{**}p<0.005$.

mice exhibited AKI, as evidenced by significantly reduced renal N-cadherin (Figure 3A), slightly decreased renal E-cadherin (Figure 3A), and markedly elevated renal Dkk3 levels (Figure 3B). Interestingly, L-G6PC1-high mice showed statistically higher N-cadherin expression compared to L-G6PC1-low mice (Figure 3A), suggesting that hepatic G6Pase-α expression may influence N-cadherin levels. Renal connective tissue growth factor (CTGF), which increases during tubular epithelial cell injury [30, 31], was similarly elevated in both groups, regardless of hepatic G6Pase-α expression levels. A similar trend was observed for Dkk3 (Figure 3B).

3.4 | Renal Fibrosis in L-G6PC1-Low and L-G6PC1-High Mice

We previously demonstrated that the kidneys of 3-week-old *G6pc−/− mice* exhibit impaired gluconeogenesis, altered glucose reabsorption, AKI, and early signs of fibrosis mediated by activation of the Wnt-β-catenin signaling pathway [13]. This pathway regulates the expression of various downstream profibrotic mediators [32–34]. In the canonical Wnt/β-catenin pathway, β-catenin is activated through dephosphorylation and translocated to the nucleus, where it forms a transcriptionally active complex with TCF/LEF (T-cell factor/lymphoid enhancer-binding factor) and co-activators to drive Wnt target gene expression [33, 34]. Both L-G6PC1-low and L-G6PC1-high mice displayed elevated renal levels of total and active β-catenin compared to controls (Figure 3C). However, the increase in total β-catenin was significantly attenuated in L-G6PC1-high mice compared to L-G6PC1-low mice, suggesting that increasing liver G6Pase-α expression may modulate total β-catenin levels in the kidney. The active β-catenin demonstrated a similar trend, although the difference between the expression in L-G6PC1-high and L-G6P-low mice did not reach statistical significance (Figure 3C). Visually, immunohistochemical analysis using an antibody against active β-catenin, combined with hematoxylin nuclear

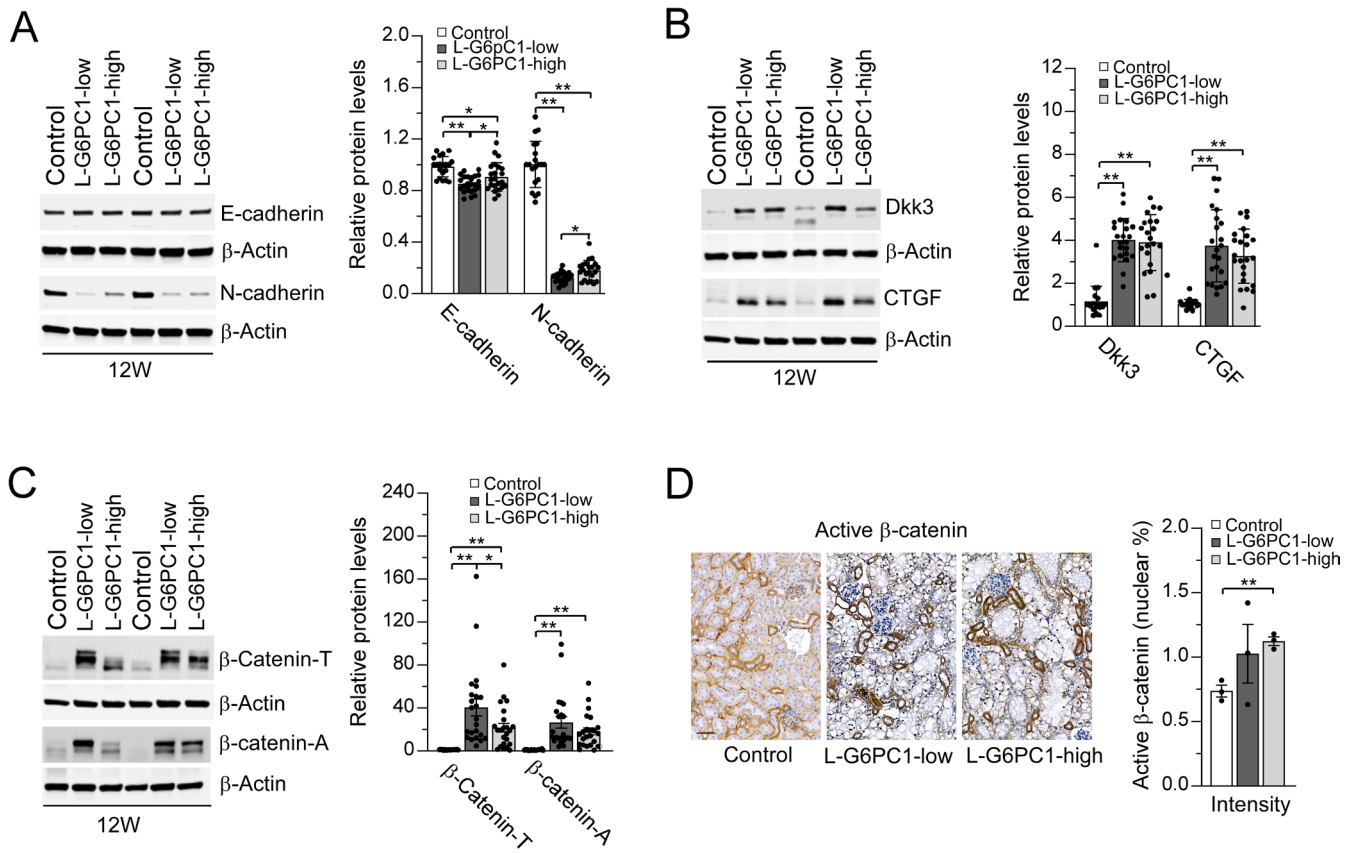

FIGURE 3 | Assessment of kidney AKI and fibrosis in L-G6PC1-low and L-G6PC1-high mice. L-G6PC1-low and L-G6PC1-high mice were generated from *G6pc*−/− mice and analyzed at 12 weeks of age. Age-matched *G6pc*+/+ and *G6pc*+/− mice with a similar phenotype served as controls. (A) Western-blot analyzes and quantitation of renal levels of E-cadherin and N-cadherin in control ($n = 20$), L-G6PC1-low ($n = 23$), and L-G6PC1-high ($n = 23$) mice. (B) Western-blot analyzes and quantitation of renal levels of Dkk3 and CTGF in control ($n = 20$), L-G6PC1-low ($n = 23$), and L-G6PC1-high ($n = 23$) mice. (C) Western-blot analyzes and quantitation of renal levels of total (β-catenin-T) and active, dephosphorylated (β-catenin-A) β-catenin in control ($n = 20$), L-G6PC1-low ($n = 23$), and L-G6PC1-high ($n = 23$) mice. For Western-blot analyzes, densitometric quantification was performed and normalized against β-Actin. Values represent the mean ± SEM. $^*p < 0.05$, $^{**}p < 0.005$. (D) Immunohistochemical analysis of renal levels of active β-catenin. Scale bar, 50 μm. (E) Quantitation of renal levels of nuclear localized active β-catenin in control ($n = 3$), L-G6PC1-low ($n = 3$), and L-G6PC1-high ($n = 3$) mice. Kidney sections were immunostained with HRP-labeled anti-active β-catenin and the nuclei counterstained with hematoxylin. Images were digitized using the Motic EasyScan Infinity 60 scanner and analyzed with QuPath software (v0.4.3). Multiple annotations were selected across the entire renal cortex. The *Nucleus DAB OD mean* scoring method [19] was used to identify moderate and strong optical density thresholds for nuclear-stained β-catenin.

counterstaining suggested that control mice exhibited diffuse cytoplasmic β-catenin staining in the renal tubules, with little nuclear β-catenin, while both L-G6PC1-low and L-G6PC1-high mice showed increased nuclear localization of β-catenin (Figure 3D). While the power of $n = 3$ is low for the L-G6PC1-low sample, quantitative analysis of nuclear staining intensity supports the visual observations (Figure 3E).

Genes in the renin-angiotensin system (RAS), which promote renal fibrosis and damage, are targets of Wnt/β-catenin signaling [32]. Renin, an aspartic protease, catalyzes the rate-limiting step of RAS activation by cleaving a 10-amino acid angiotensin I (Ang I) peptide from the N-terminus of angiotensinogen (AGT) [35]. In 12-week-old L-G6PC1-low and L-G6PC1-high mice, renal renin levels were elevated compared to controls but did not correlate with liver G6Pase-α activity levels (Figure 4A). Interestingly, while L-G6PC1-low mice exhibited increased renal AGT levels, AGT in L-G6PC1-high mice was statistically similar to those of age-matched controls (Figure 4A). This suggests that augmentation of liver G6Pase-α activity in *G6pc*−/− mice prevents the elevation of renal AGT levels.

The transcription factor Snail1, a target of Wnt/β-catenin signaling, plays a key role in fibroblast activation [36]. Its activation induces a partial epithelial-mesenchymal transition (EMT), promoting epithelial cell de-differentiation and renal fibrosis [36]. In 12-week-old L-G6PC1-high and L-G6PC1-low mice, renal Snail1 levels were elevated compared to controls but did not correlate with liver G6Pase-α activity (Figure 4B). Renal fibrosis is also marked by increased expression of α-smooth muscle actin (α-SMA) [37] and extracellular matrix (ECM) proteins such as collagens [38]. Both groups of mice exhibited significantly elevated renal levels of α-SMA (Figure 4B), collagen I-α1 (Col-Iα1) (Figure 5A), and collagen IV (Col-IV) (Figure 5A) compared to controls, with no correlation to liver G6Pase-α activity. Supporting this, Masson's

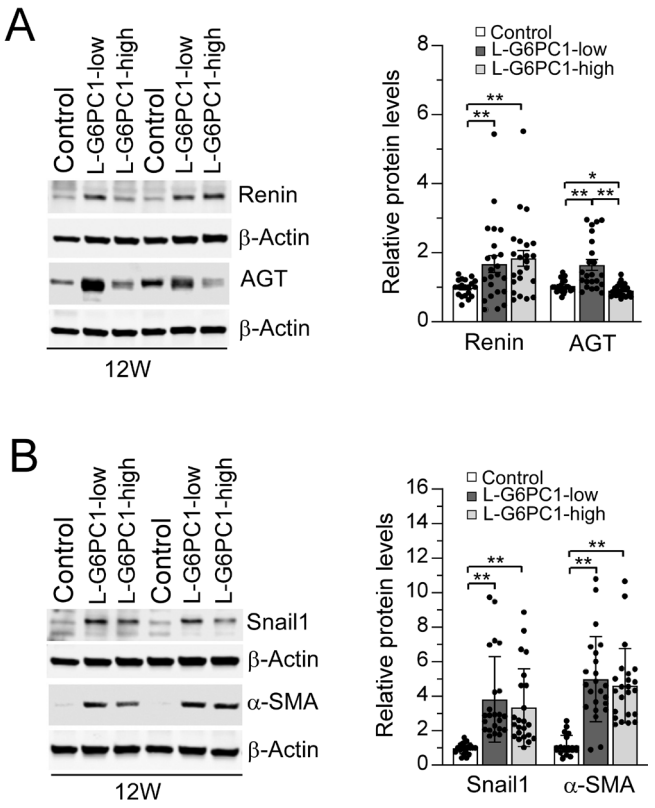

FIGURE 4 | Assessment of renal levels of renin, AGT, Snail1, and α-SMA in L-G6PC1-low and L-G6PC1-high mice. L-G6PC1-low and L-G6PC1-high mice were generated from *G6pc*−/− mice and analyzed at 12 weeks of age. Age-matched *G6pc*+/+ and *G6pc*+/− mice with a similar phenotype served as controls. (A) Western-blot analyzes and quantitation of renal levels of renin and AGT in control ($n = 20$), L-G6PC1-low ($n = 23$), and L-G6PC1-high ($n = 23$) mice. (B) Western-blot analyzes and quantitation of renal levels of Snail1 and α-SMA in control ($n = 20$), L-G6PC1-low ($n = 23$), and L-G6PC1-high ($n = 23$) mice. Densitometric quantification was performed and normalized against β-Actin. Values represent the mean ± SEM. $^{*}p < 0.05$, $^{**}p < 0.005$.

trichrome staining showed no apparent difference in kidney fibrosis between L-G6PC1-high and L-G6PC1-low mice (Figure 5B).

Serum biomarkers of renal function include cystatin C, BUN, and creatinine [14]. Serum cystatin C levels were significantly elevated in L-G6PC1-low mice but remained within the normal range in L-G6PC1-high mice, comparable to controls (Figure 5C). Similarly, while serum BUN levels were elevated in both L-G6PC1-low and L-G6PC1-high mice, the increase in L-G6PC1-high mice was significantly attenuated (Figure 5C). These findings suggest that higher hepatic G6Pase-α expression (L-G6PC1-high) may normalize cystatin C levels and partially normalize BUN levels. Serum creatinine levels were elevated in both groups, irrespective of hepatic G6Pase-α expression (Figure 5C). Overall, although both groups exhibited early signs of renal dysfunction, L-G6PC1-high mice showed less compromised glomerular filtration. This suggests that higher hepatic G6Pase-α expression mitigates early renal disease in GSD-Ia.

4 | Discussion

Human patients with GSD-Ia face a long-term risk of renal disease [1–3] and rely on strict dietary therapies [4–6] to manage their conditions. Current gene augmentation (NCT05139316) [7, 15, 16] and genome editing (NCT06735755) [7, 8] therapies in clinical trials are liver-directed. While these approaches show promise in improving metabolic control, it remains unclear whether enhanced liver function can also benefit kidney function or mitigate early nephropathy, which might also delay the progression of kidney disease. Clinical studies on standard dietary therapies suggest that strict metabolic control can improve renal function [11], but the underlying mechanisms in GSD-Ia remain poorly understood. In previous studies using the *G6pc*−/− mouse model [12], which mimics GSD-Ia pathophysiology, we identified renal fibrosis mediated by Wnt/β-catenin signaling activation as a key contributor to GSD-Ia nephropathy [13]. However, due to hypoglycemic seizures and early mortality, *G6pc*−/− mice are unsuitable for long-term kidney studies [12]. While a kidney-specific G6Pase-α knockout mouse strain has been reported by Clar et al. [39], it retains 50% kidney G6Pase-α activity, making it unsuitable for studying autosomal recessive GSD-Ia nephropathy.

To better understand the impact of kidney-specific G6PC1 deficiency, we developed a novel strategy using liver-specific gene augmentation of *G6pc*−/− mouse [9], creating a liver G6Pase-α positive, kidney G6Pase-α-null mouse (L-G6PC1/K^{null}) [13]. Since we can reproducibly titrate the level of G6Pase-α restoration in the liver using a rAAV-G6PC1 vector [7, 9, 15, 16] we have examined two different conditions in which we restored either 2% (L-G6PC1-low) or 86% (L-G6PC1-high) of control hepatic G6Pase-α activity. This strategy enables the exploration of how liver G6Pase-α activity affects kidney function in the context of kidney G6Pase-α deficiency, advancing the understanding of how liver-directed gene therapy might influence nephropathy in GSD-Ia.

In this study, we showed that 12-week-old L-G6PC1-low and L-G6PC1-high mice displayed impaired renal glucose homeostasis, altered renal glucose reabsorption, AKI, and renal fibrosis mediated by activation of renal Wnt/β-catenin signaling as was previously observed in 3-week-old *G6pc*−/− mice [13]. However, the severity of renal impairments on glucose homeostasis and reabsorption was influenced by the level of G6Pase-α activity restored in the liver, with L-G6PC1-high mice showing less severe renal dysfunction compared to L-G6PC1-low mice. Renal function, assessed through serum marker analysis [14], revealed that serum cystatin C levels in the L-G6PC1-high mice were comparable to control mice, indicating improved glomerular filtration. While both L-G6PC1-low and L-G6PC1-high mice had higher serum BUN levels than the control mice, the increase in serum BUN was significantly less pronounced in the L-G6PC1-high mice. This suggests that higher liver G6Pase-α activity provided by liver-directed gene therapy may be able to alleviate renal dysfunction and have the potential to improve kidney function in GSD-Ia.

The 12-week-old L-G6PC1-low and L-G6PC1-high mice, which lack renal G6Pase-α and are unable to produce renal glucose via gluconeogenesis, exhibited impaired renal glucose

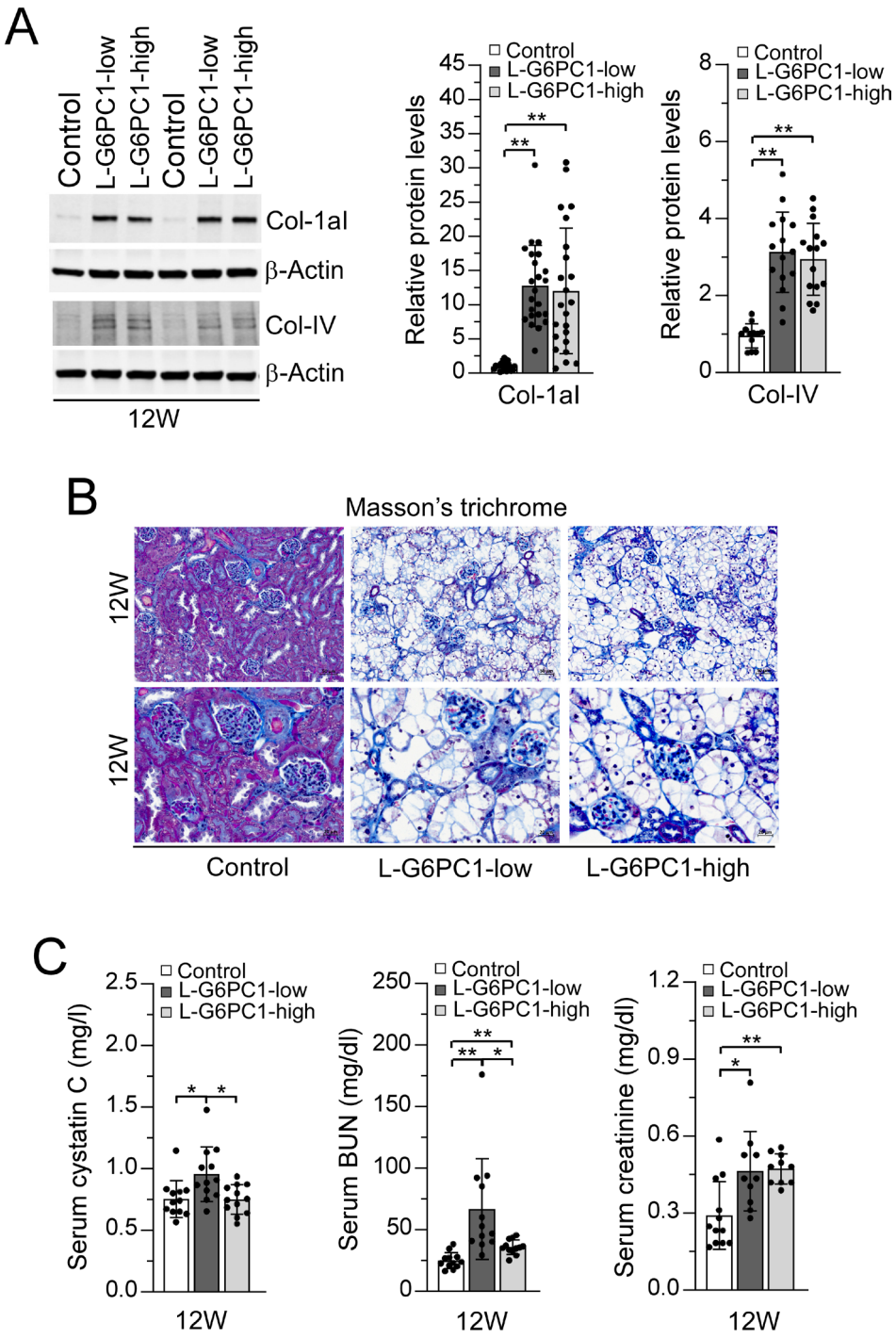

FIGURE 5 | Assessment kidney fibrosis and dysfunction in L-G6PC1-low and L-G6PC1-high mice. L-G6PC1-low and L-G6PC1-high mice were generated from *G6pc*−/− mice and analyzed at 12 weeks of age. Age-matched *G6pc*+/+ and *G6pc*+/− mice with a similar phenotype served as controls. (A) Western-blot analyzes and quantification of renal levels of Col-1α1 and Col-IV in control ($n = 20$), L-G6PC1-low ($n = 23$), and L-G6PC1-high ($n = 23$) mice. Densitometric quantification was performed and normalized against β-Actin. (B) Masson's trichrome staining of kidney sections in 12-week-old control, L-G6PC1-low, and L-G6PC1-high mice at magnifications of ×200 (top panels, Scale bar, 50 μm) and ×400 (lower panels, Scale bar, 20 μm). Representative sets of staining are shown. Renal fibrosis in mice was shown by the blue colored staining of the collagen fibers. (C) Serum levels of cystatin C, BUN, and creatinine in 12-week-old control ($n = 6$), L-G6PC1-low ($n = 6$), and L-G6PC1-high ($n = 6$) mice. Values represent the mean ± SEM. $^{*}p < 0.05$, $^{**}p < 0.005$.

homeostasis. Consequently, both groups had significantly lower serum glucose levels compared to the control mice. However, blood glucose levels were higher in the L-G6PC1-high mice than in the L-G6PC1-low mice, and serum triglyceride and lactate levels were elevated only in the L-G6PC1-low mice, suggesting that higher liver G6Pase-α activity could improve glucose homeostasis. This improvement in glucose homeostasis in L-G6PC1-high mice was further demonstrated by reduced glycogen accumulation in the kidneys, improved nephromegaly, and lower renal lactate levels compared to the

L-G6PC1-low mice. Additionally, lipid accumulation in renal glomerular and tubular cells, which is commonly associated with renal injury that contributes to nephropathy [17, 18], was observed primarily in the L-G6PC1-low mice. Renal triglyceride levels in the L-G6PC1-high mice were comparable to those of the control mice. This suggests that restoring high levels of liver G6Pase-α activity helps reduce early renal damage and offers hope that it may be possible to modulate long-term progression of kidney injury in GSD-Ia.

Both L-G6PC1-low and L-G6PC1-high mice at age 12 weeks exhibited altered renal glucose reabsorption. The renal cortex reabsorbs 90% of urinary glucose via SGLT2-mediated glucose transport across the apical membrane while GLUT2 mediates most of the glucose release back into the blood stream [24–26]. Both mouse groups showed reduced renal levels of SGLT2 and increased levels of GLUT2, indicating impaired glucose reabsorption. However, in the L-G6PC1-high mice, these changes were normalized, with SGLT2 levels restored and GLUT2 levels returning closer to control levels. This suggests that higher liver G6Pase-α expression improves renal glucose reabsorption. Additionally, renal levels of total β-catenin were significantly reduced in L-G6PC1-high mice compared to L-G6PC1-low mice, suggesting a reduction in Wnt/β-catenin signaling. However, the difference in active β-catenin levels between the two groups was not statistically significant, which may explain why the renal fibrosis observed in both groups was similar. This suggests that while liver G6Pase-α expression can improve glucose reabsorption and reduce total β-catenin levels, it does not fully resolve the renal fibrosis associated with GSD-Ia nephropathy.

The 12-week-old L-G6PC1-low and L-G6PC1-high mice exhibited elevated renal levels of renin, an aspartyl-protease that catalyzes cleavage of the 10-amino acid peptide Ang I from the N-terminus of AGT [35]. Ang I is proteolytically cleaved by angiotensin-converting enzyme to release the biologically active peptide Ang II. Both renin and AGT are target genes of Wnt/β-catenin signaling [32]. However, renal levels of AGT were only increased in the L-G6PC1-low mice. This suggests that high levels of liver G6Pase-α activity, as seen in L-G6PC1-high mice, prevent the rise in renal levels of AGT and the Ang peptides, which are known to mediate renal fibrosis. While AGT is primarily known for its role in producing Ang II, studies have also shown that AGT can have Ang II-independent effects, such as modulating body weight gain and liver steatosis through a des(angiotensin I)AGT variant [40, 41]. However, whether the reduced renal AGT levels in the L-G6PC1-high mice contribute to their healthier phenotype compared to the L-G6PC1-low mice remains unclear. This presents an area for further investigation to understand the broader effects of AGT modulation in GSD-Ia nephropathy.

Studies have shown that GSD-Ia patients who receive a functional liver transplant achieve normal metabolic control and fasting tolerance [42, 43]. However, whether liver transplantation provides renal protection remains controversial. Boers et al. [42], reviewed long-term outcomes of liver transplantation in 58 GSD-Ia patients, with a median transplantation age of 20 years, who underwent the procedure between 1982 and 2012. Their study found that all patients experienced improved metabolic control and normal fasting tolerance post-transplantation. However, renal failure was the most common complication occurring in 24% of patients. Renal function improved in four patients with pre-transplantation renal dysfunction, though three of these four had undergone combined liver-kidney transplantation. In contrast, Chan et al. [43], reported long-term outcomes in 8 GSD-Ia patients who underwent liver transplantation at a median age of 9 years, with a follow-up period of 15 years. Their findings indicated that renal function post-transplantation remained well-preserved in most patients. Notably, initiation of cornstarch dietary therapy before preschool age [43], followed by liver transplantation, was associated with favorable renal outcomes, suggesting that good early metabolic control enhances prognosis after transplantation. The differing conclusions between the two studies may be attributed to differences in the median age at transplantation, 20 years in the Boers et al. study [42] versus 9 years in the Chan et al. study [43], as well as prior dietary management. Strict dietary therapy has been shown to slow renal disease progression [11]. These findings suggest that early intervention with effective dietary management may also help mitigate renal dysfunction following GSD-Ia gene therapy.

In summary, preclinical studies have shown that liver-specific G6PC1 gene augmentation [7, 9, 15, 16] and gene editing [7, 8] improve survival and significantly alleviate liver dysfunction in GSD-Ia mice. Clinical trials of these approaches are promising and may offer a more effective therapy for GSD-Ia patients. However, their impact on GSD-Ia nephropathy remains unclear. In this study, we utilized the novel L-G6PC1/K^{null} mouse model [13] to investigate the long-term effects of restoring liver G6Pase-α function on the pathophysiology of GSD-Ia nephropathy. Our findings indicate that liver-directed gene augmentation may benefit the kidney by improving renal function, but it does not appear to prevent renal fibrosis. Future studies will extend the investigation beyond 12 weeks to a significantly longer timeframe (~52 weeks) and explore varying levels of liver G6Pase-α expression to gain deeper insights and guide future clinical applications. Additionally, we aim to explore alternative strategies that facilitate direct transduction of the kidney with rAAV-G6PC1 [44, 45] and assess their efficacy in correcting renal dysfunction in GSD-Ia, ultimately striving to further improve patient outcomes.

Author Contributions

C.L. performed the experiments, analyzed the data, and wrote the paper; K.P., L.Z., H.D.C., and I.A. performed the experiments, analyzed the data, and edited the manuscript; M.F.S. performed pathological analysis and edited the manuscript; B.C.M. analyzed the data and edited the manuscript; J.Y.C. designed the research, acquired the funding, analyzed the data, wrote the paper, and is the GUARANTOR for the article.

Consent

The authors have nothing to report.

Conflicts of Interest

The authors declare no conflicts of interest.

Data Availability Statement

The data that support the findings of this study are available from the corresponding author upon reasonable request.

References

1. J. Y. Chou, H. S. Jun, and B. C. Mansfield, "Glycogen Storage Disease Type I and G6Pase-Beta Deficiency: Etiology and Therapy," *Nature Reviews Endocrinology* 6, no. 12 (2010): 676–688.

2. J. Y. Chou, H. S. Jun, and B. C. Mansfield, "Type I Glycogen Storage Diseases: Disorders of the Glucose-6-Phosphatase/Glucose-6-Phosphate Transporter Complexes," *Journal of Inherited Metabolic Disease* 38, no. 3 (2015): 511–519.

3. P. S. Kishnani, S. L. Austin, J. E. Abdenur, et al., "Diagnosis and Management of Glycogen Storage Disease Type I: A Practice Guideline of the American College of Medical Genetics and Genomics," *Genetics in Medicine* 16, no. 11 (2014): e1.

4. H. L. Greene, A. E. Slonim, J. A. O'Neill, Jr., and I. M. Burr, "Continuous Nocturnal Intragastric Feeding for Management of Type 1 Glycogen-Storage Disease," *New England Journal of Medicine* 294, no. 8 (1976): 423–425.

5. Y. T. Chen, M. Cornblath, and J. B. Sidbury, "Cornstarch Therapy in Type I Glycogen Storage Disease," *New England Journal of Medicine* 310, no. 3 (1984): 171–175.

6. K. M. Ross, I. A. Ferrecchia, K. R. Dahlberg, M. Dambska, P. T. Ryan, and D. A. Weinstein, "Dietary Management of the Glycogen Storage Diseases: Evolution of Treatment and Ongoing Controversies," *Advances in Nutrition* 11, no. 2 (2020): 439–446.

7. J. Y. Chou and B. C. Mansfield, "Gene Therapy and Genome Editing for Type I Glycogen Storage Diseases," *Frontiers in Molecular Medicine* 3 (2023): 1167091, https://doi.org/10.3389/fmmed.2023.1167091.

8. I. Arnaoutova, Y. Aratyn-Schaus, L. Zhang, et al., "Base-Editing Corrects Metabolic Abnormalities in a Humanized Mouse Model for Glycogen Storage Disease Type-Ia," *Nature Communications* 15, no. 1 (2024): 9729.

9. Y. M. Lee, C. J. Pan, D. D. Koeberl, B. C. Mansfield, and J. Y. Chou, "The Upstream Enhancer Elements of the *G6PC* Promoter Are Critical for Optimal G6PC Expression in Murine Glycogen Storage Disease Type Ia," *Molecular Genetics and Metabolism* 110, no. 3 (2013): 275–280.

10. M. Hosseini-Kharat, K. E. Bremmell, and C. A. Prestidge, "Why Do Lipid Nanoparticles Target the Liver? Understanding of Biodistribution and Liver-Specific Tropism," *Molecular Therapy - Methods & Clinical Development* 33, no. 1 (2025): 101436.

11. G. O. Okechuku, L. R. Shoemaker, M. Dambska, L. M. Brown, J. Mathew, and D. A. Weinstein, "Tight Metabolic Control Plus ACE Inhibitor Therapy Improves GSD I Glomerulopathy," *Journal of Inherited Metabolic Disease* 40, no. 5 (2017): 703–708.

12. K. J. Lei, H. Chen, C. J. Pan, et al., "Glucose-6-Phosphatase Dependent Substrate Transport in the Glycogen Storage Disease Type-1a Mouse," *Nature Genetics* 13, no. 2 (1996): 203–209.

13. C. Lee, K. Pratap, L. Zhang, et al., "Inhibition of Wnt/β-Catenin Signaling Reduces Renal Fibrosis in Murine Glycogen Storage Disease Type Ia," *Biochimica et Biophysica Acta-Molecular Basis of Disease* 1870, no. 1 (2024): 166874.

14. S. Gowda, P. B. Desai, S. S. Kulkarni, et al., "Markers of Renal Function Tests," *North American Journal of Medical Sciences* 2, no. 4 (2010): 170–173.

15. Y. M. Lee, H. S. Jun, C. J. Pan, et al., "Prevention of Hepatocellular Adenoma and Correction of Metabolic Abnormalities in Murine Glycogen Storage Disease Type Ia by Gene Therapy," *Hepatology* 56, no. 5 (2012): 1719–1729.

16. G. Y. Kim, Y. M. Lee, J. H. Kwon, et al., "Glycogen Storage Disease Type Ia Mice With Less Than 2% of Normal Hepatic Glucose-6-Phosphatase-α Activity Restored Are at Risk of Developing Hepatic Tumors," *Molecular Genetics and Metabolism* 120, no. 3 (2017): 229–234.

17. R. A. Zager, A. C. M. Johnson, and S. Y. Hanson, "Renal Tubular Triglyceride Accumulation Following Endotoxic, Toxic, and Ischemic Injury," *Kidney International* 67, no. 1 (2005): 111–121.

18. J. M. Weinberg, "Lipotoxicity," *Kidney International* 70, no. 9 (2006): 1560–1566.

19. P. Bankhead, M. B. Loughrey, J. A. Fernández, et al., "QuPath: Open Source Software for Digital Pathology Image Analysis," *Scientific Reports* 7, no. 1 (2017): 16878.

20. J. E. Gerich, "Role of the Kidney in Normal Glucose Homeostasis and in the Hyperglycemia of Diabetes Mellitus: Therapeutic Implications," *Diabetes Medicine* 27, no. 2 (2010): 136–142.

21. M. Alsahli and J. E. Gerich, "Renal Glucose Metabolism in Normal Physiological Conditions and in Diabetes," *Diabetes Research and Clinical Practice* 133 (2017): 1–9.

22. J. H. Cho, Y. M. Lee, S. H. Bae, and J. Y. Chou, "Activation of Tumor-Promoting Pathways Implicated in Hepatocellular Adenoma/Carcinoma, a Long-Term Complication of Glycogen Storage Disease Type Ia," *Biochemical and Biophysical Research Communications* 522, no. 1 (2020): 1–7.

23. G. Y. Kim, Y. M. Lee, J. H. Cho, et al., "Mice Expressing Reduced Levels of Hepatic Glucose-6-Phosphatase-α Activity Do Not Develop Age-Related Insulin Resistance and Obesity," *Human Molecular Genetics* 24, no. 18 (2015): 5115–5125.

24. B. D. Shepard and J. L. Pluznick, "Saving the Sweetness: Renal Glucose Handling in Health and Disease," *American Journal of Physiology Renal Physiology* 313, no. 1 (2017): F55–F61.

25. C. Ghezzi, D. D. F. Loo, and E. M. Wright, "Physiology of Renal Glucose Handling via SGLT1, SGLT2 and GLUT2," *Diabetologia* 61, no. 10 (2018): 2087–2097.

26. V. Vallon, "Glucose Transporters in the Kidney in Health and Disease," *Pflügers Archiv* 472, no. 9 (2020): 1345–1370.

27. J. Nürnberger, T. Feldkamp, R. Kavapurackal, et al., "N-Cadherin Is Depleted From Proximal Tubules in Experimental and Human Acute Kidney Injury," *Histochemistry and Cell Biology* 33, no. 6 (2010): 641–649.

28. R. L. Chevalier, "The Proximal Tubule Is the Primary Target of Injury and Progression of Kidney Disease: Role of the Glomerulotubular Junction," *American Journal of Physiology. Renal Physiology* 311, no. 1 (2016): F145–F161.

29. X. Fang, J. Hu, Y. Chen, W. Shen, and B. Ke, "Dickkopf-3: Current Knowledge in Kidney Diseases," *Frontiers in Physiology* 11 (2020): 533344.

30. Y. Ramazani, N. Knops, M. A. Elmonem, et al., "Connective Tissue Growth Factor (CTGF) From Basics to Clinics," *Matrix Biology* 68-69 (2018): 44–66.

31. Q. Yin and H. Liu, "Connective Tissue Growth Factor and Renal Fibrosis," *Advances in Experimental Medicine and Biology* 1165 (2019): 365–380.

32. L. Zhou, Y. Li, S. Hao, et al., "Multiple Genes of the Renin-Angiotensin System Are Novel Targets of Wnt/β-Catenin Signaling," *Journal of the American Society of Nephrology* 26, no. 1 (2015): 7–120.

33. Y. Zuo and Y. Liu, "New Insights Into the Role and Mechanism of Wnt/β-Catenin Signaling in Kidney Fibrosis," *Nephrology* 23, no. Suppl 4 (2018): 38–43.

34. S. J. Schunk, J. Floege, D. Fliser, and T. Speer, "WNT-β-Catenin Signalling—A Versatile Player in Kidney Injury and Repair," *Nature Reviews Nephrology* 17, no. 3 (2021): 172–184.

35. T. Yang and C. Xu, "Physiology and Pathophysiology of the Intrarenal Renin-Angiotensin System: An Update," *Journal of the American Society of Nephrology* 28, no. 4 (2017): 1040–1049.

36. M. T. Grande, B. Sánchez-Laorden, C. López-Blau, et al., "Snail1-Induced Partial Epithelial-To-Mesenchymal Transition Drives Renal Fibrosis in Mice and Can Be Targeted to Reverse Established Disease," *Nature Medicine* 21, no. 9 (2015): 989–997.

37. R. D. Bülow and P. Boor, "Extracellular Matrix in Kidney Fibrosis: More Than Just a Scaffold," *Journal of Histochemistry and Cytochemistry* 67, no. 9 (2019): 643–661.

38. B. D. Humphreys, "Mechanisms of Renal Fibrosis," *Annual Review of Physiology* 80 (2018): 309–326.

39. J. Clar, B. Gri, J. Calderaro, et al., "Targeted Deletion of Kidney Glucose-6 Phosphatase Leads to Nephropathy," *Kidney Internal* 86, no. 4 (2014): 747–756, https://doi.org/10.1038/ki.2014.102.

40. C. Wu, H. Lu, L. A. Cassis, and A. Daugherty, "Molecular and Pathophysiological Features of Angiotensinogen: A Mini Review," *North American Journal of Medical Sciences* 4, no. 4 (2011): 183–190.

41. H. Lu, C. Wu, D. A. Howatt, et al., "Angiotensinogen Exerts Effects Independent of Angiotensin II," *Arteriosclerosis, Thrombosis, and Vascular Biology* 36, no. 2 (2016): 256–265.

42. S. J. B. Boers, G. Visser, P. G. P. A. Smit, and S. A. Fuchs, "Liver Transplantation in Glycogen Storage Disease Type I," *Orphanet Journal of Rare Diseases* 9 (2014): 47.

43. Y.-C. Chan, K.-M. Liu, C.-L. Chen, et al., "Modifiable Factors Affecting Renal Preservation in Type I Glycogen Storage Disease After Liver Transplantation: A Single-Center Propensity-Match Cohort Study," *Orphanet Journal of Rare Diseases* 16, no. 1 (2021): 423.

44. C. J. Rocca, S. N. Ur, F. Harrison, and S. Cherqui, "rAAV9 Combined With Renal Vein Injection Is Optimal for Kidney-Targeted Gene Delivery: Conclusion of a Comparative Study," *Gene Therapy* 21, no. 6 (2014): 618–628.

45. T. Furusho, R. Das, H. Hakui, et al., "Enhancing Gene Transfer to Renal Tubules and Podocytes by Context-Dependent Selection of AAV Capsids," *Nature Communications* 15, no. 1 (2024): 10728.